Supporting Information for

Rapid ultrasensitive detection of levamisole and mebendazole residues in meat products based on intelligent nanozyme-imprinted fluorescence microfluidic sensor

Qiuyu Wu[a], Zhihui Liao[a], Yujin Ouyang[b], Ao Ma[a], Zhaoxia Yang[b], Zhaohui Zhang[a, b, c]

[a]College of Pharmaceutical Science, Jishou University, Hunan 416000, PR China

[b]College of Chemistry and Chemical Engineering, Jishou University, Hunan 416000, PR China

[c]Key Laboratory of Medicinal Resources Chemistry and Pharmacology in Wuling Mountainous of Hunan Province College, Jishou University, Jishou 416000, PR China

E-mail: zhaohuizhang77@163.com (Z. H. Zhang)

1. Experimental Section

1.1 Reagents and instruments

4,4,4-(Porphine-5,10,15,20-tetrayl) tetrakis (benzoic acid) (TCCP) (≥97%), $ZrOCl_2 \cdot 8H_2O$ (≥99.99%), benzoic acid (BA) (≥99%), $ZrCl_4$ (≥98%), 2-aminoterephthalic acid (2-NH_2-1,4-BDC) (≥98%), 3,3',5,5'-tetramethylbenzidine (TMB) (≥99%), N,N-dimethylformamide (DMF) (≥99.5%), o-phenylenediamine (OPD) (≥99.5%), ammonia solution (≥99.999%), acetic acid (HAc) (≥99.5%), ethanol (≥95%), (3-aminopropyl) triethoxysilane (APTES) (≥98%), hydrogen peroxide solution (H_2O_2), mebendazole (MBZ) (≥99%), levamisole (LMS) (≥99%), disodium hydrogen phosphate-diethylamine, methanol (CH_3OH) (≥99%), ammonium dihydrogen phosphate-triethylamine, acetonitrile (C_2H_3N) (≥99%) and hydrochloride were obtained from Aladdin Biochemical Technology Co., Ltd. (Shanghai, China). Tetraethyl orthosilicate (TEOS) (≥98%) was purchased from Shanghai Macklin Biochemical Co., Ltd. Ultra-pure water was used throughout the experiments.

All fluorescence data were measured using an F-7000 fluorescence spectrometer (Hitachi, Japan). The morphologic images of materials were obtained by German ZEISS Sigma 300 scanning electron microscope. Ultraviolet visible (UV-Vis) absorption spectra were collected by a UV-1780 spectrophotometer (Shimadzu, Japan). X-ray diffraction (XRD) data were recorded by a Dandong Tongda (TD3500) X-ray diffractometer (China). Fourier-transform infrared (FT-IR) spectra were recorded using a Nicolet iS10 Fourier transform infrared spectrometer (Thermo Fisher,

USA). X-ray photoelectron spectroscopy (XPS) was provided by Thermo Scientific K-Alpha device (America). In addition, the Bruker ESP 300E electron spin Resonance (EPR) spectrometer was used to collect the electron spin resonance spectrum of the capture-free radical signal.

1.2 Preparation of UiO-66-NH_2 and PCN-224

The preparation of UiO-66-NH_2 was based on previous method with slight modifications [51]. First, 0.699 g of $ZrCl_4$ solid and 0.543 g of 2-NH_2-1,4-BDC were dissolved in 18 mL of DMF. Then, 7.5 mL of HAc was added, and the mixture solution was stirred for 30 minutes. Slowly transferred to a 50-mL autoclave, the above mixture was reacted at 120 °C for 24 hours. Cooled at room temperature, the solution was centrifuged at 5400 rpm for 3 minutes. The precipitate was successively washed twice with DMF and methanol to remove unreacted raw materials and by-products. Finally, the purified material was dried in a drying oven at 60 °C for 48 hours to obtain light red powdered UiO-66-NH_2, which was stored in a desiccator for later use.

The synthesis of PCN-224 was performed based on previous method with some modifications [52]. Firstly, 60 mg of TCPP, 180 mg of $ZrOCl_2 \cdot 8H_2O$, and 1.68 g of BA were dissolved in 60 mL of DMF. The mixture was magnetically stirred at 300 rpm for 5 hours to ensure sufficient reaction. Cooled to room temperature, the porous metal-organic framework material PCN-224 was collected by centrifugation at 5400 rpm for 3 minutes. Repeatedly washed with DMF for 3 times, the centrifuged precipitate was dried in a vacuum oven at 60°C for 12 hours. Finally, a purple

crystalline powder was stored in a desiccator for later use.

1.3 Preparation of UiO-66-NH_2@MIP/PCN-224@MIP 3D μPAD

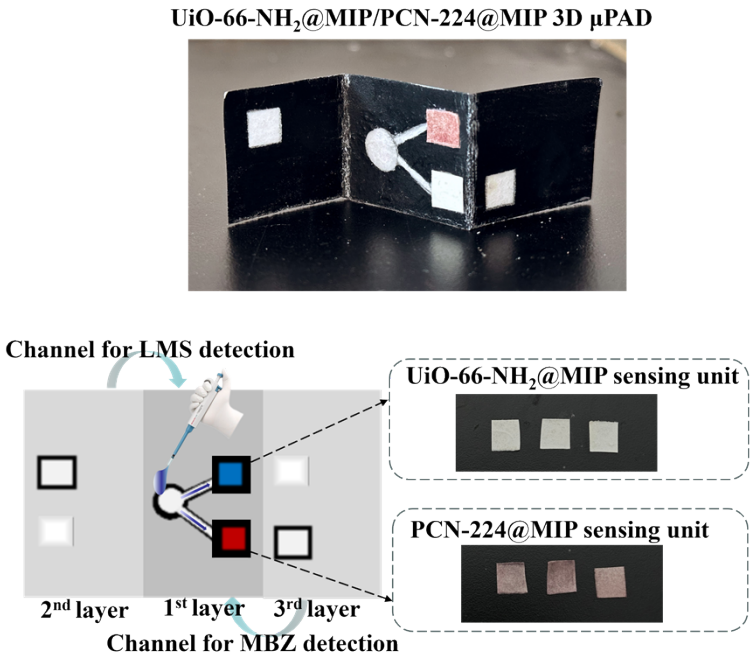

Scheme S1 Photograph of the 3D μPAD with dual detection channels.

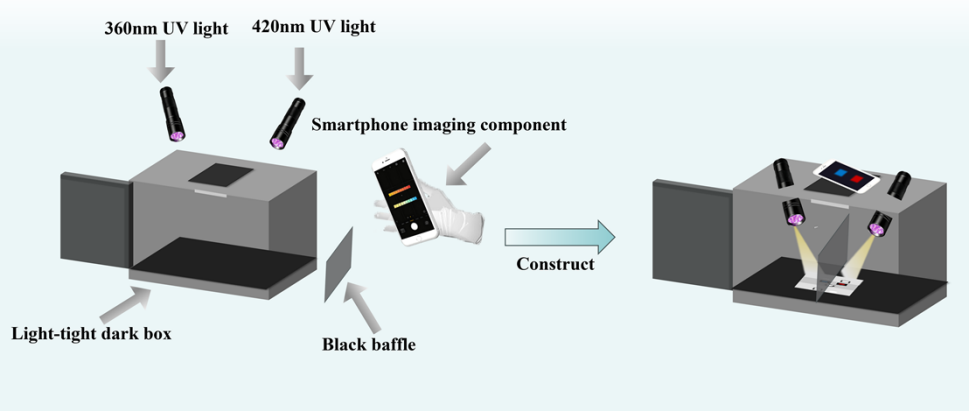

Scheme S2 Development of a dual-excitation fluorescence visual detection platform.

1.4 Peroxidase-like activity assay

Briefly, under the condition of fixing the concentrations of other substances, the

catalytic kinetics of enzyme-like substances were tested by changing the concentration of H_2O_2 or TMB. In the study of TMB, 1.0 mL of TMB (0.1-1 mM), 100 μL of H_2O_2 (0.98 mM), and 50 μL of UiO-66-NH_2 or PCN-224 aqueous dispersion (1 mg/mL) were mixed with 1.85 mL of HAc-NaAc buffer (pH=4.0). In the study of H_2O_2, 100 μL of H_2O_2 (1-10 mM), 1.0 mL of TMB (5 mM), and 50 μL of UiO-66-NH_2 or PCN-224 aqueous dispersion (1 mg/mL) were mixed with 1.85 mL of HAc-NaAc buffer (pH=4.0). After reaction for 6 minutes, the absorbance value at 652 nm was measured using an ultraviolet spectrophotometer. The kinetic parameters were calculated according to the Michaelis-Menten equation:

$$1/V = K_m/V_{max}[S] + 1/V_{max}$$

where V is the initial reaction rate, V_{max} is the maximum reaction rate, [S] is the substrate concentration, and K_m is the Michaelis constant.

1.5 Pretreatment and detection of actual samples

Spiked recovery experiments toward LMS and MBZ were performed in beef, chicken, and egg samples purchased from a local supermarket in Jishou. The pretreatment of real samples was according with previous method [53]. Shelled eggs were homogenized with high-speed stirring to obtain a uniform emulsion free of visible particle aggregates. Beef and chicken were minced into a fine paste (particle size < 0.5 mm). Then 5 mL of 0.1 mM Na_2EDTA and 20 mL of acetonitrile containing 1% acetic acid were added, followed by vortex mixing for 3 minutes. After 4 g of anhydrous sodium carbonate and 1 g of sodium chloride were added, the mixture was vortex mixed for 3 minutes. Each sample was diluted with 300 mL of

deionized water for fluorescence analysis. All samples were respectively tested with UiO-66-NH_2@MIP/PCN-224@MIP 3D μPAD sensor and HPLC. All measurements were performed in triplicate, and the results are reported as mean ± SD (n = 3).

Code for a MATLAB program-driven smartphone to read fluorescence signals and generate color heatmaps of (B+G)/R and (B+R)/G values from fluorescence images

(1) Channel for LMS detection:

```
import numpy as np
import matplotlib.pyplot as plt
from PIL import Image, ImageDraw
from matplotlib.colors import LinearSegmentedColormap

# Open the image
img = Image.open(r' your_image')
img_resized = img.resize((12 * (img.width // 12), 5 * (img.height // 5)))
img_array = np.array(img_resized)
block_height = img_resized.height // 5
block_width = img_resized.width // 12

# Image preprocessing
rgb_values = np.zeros((5, 12, 3), dtype=int)

# Calculate the average RGB value of each grid block
for i in range (5):
    for j in range (12):
        block = img_array [i * block_height:(i + 1) * block_height, j *
block_width:(j + 1) * block_width]
        rgb_values [i, j] = block.mean(axis = (0, 1))
```

```
# Calculate (B+G)/R ratio
bg_r_ratios = (rgb_values [:, :, 1] + rgb_values [:, :, 2]) / rgb_values [:, :, 0]

# Visualization
colors = ["#FFFF00", "#6495ED"]
cmap = LinearSegmentedColormap.from_list ("custom_cmap", colors)

# Create heatmap
plt.figure(figsize = (12, 6))
plt.imshow(bg_r_ratios, aspect='auto', cmap=cmap, vmin=1.5, vmax=4)
plt.colorbar(label='(B+G)/R Value')

# Axis configuration
new_x_labels = [f"{x:.1f}" for x in np.arange(0.05, 2.8, 0.275)]
num_ticks = len(new_x_labels)
x_ticks_positions = np.linspace(0, 11, num_ticks) # Evenly distributed from 0 to 11
plt.xticks(x_ticks_positions, new_x_labels, fontsize=16, fontweight='bold')
y_labels = [1, 2, 3, 4, 5]
plt.yticks(np.arange(len(y_labels)), y_labels, fontsize=16, fontweight='bold')
plt.xlabel('LMS Concentration (μM)', fontsize=18, fontweight='bold')
plt.ylabel('Repetition', fontsize=18, fontweight='bold')
plt.title('Heatmap of (B+G)/R for LMS', fontsize=20, fontweight='bold')

# Data annotation
for i in range(bg_r_ratios.shape[0]):
    for j in range(bg_r_ratios.shape[1]):
```

```
            value = bg_r_ratios[i, j]
            plt.text(j, i, f'{value:.2f}',
                     ha='center', va='center',
                     color='black' if value < 2.75 else 'white',
fontsize=14, fontweight='bold')
plt.tight_layout()
plt.show()
```

(2) Channel for MBZ detection:

```
import numpy as np
import matplotlib.pyplot as plt
from PIL import Image, ImageDraw
from matplotlib.colors import LinearSegmentedColormap

# Open the image
img = Image.open(r' your_image')
img_resized = img.resize((12 * (img.width // 12), 5 * (img.height // 5)))
img_array = np.array(img_resized)

# Image preprocessing
block_height = img_resized.height // 5
block_width = img_resized.width // 12
rgb_values = np.zeros((5, 12, 3), dtype=int)

# Calculate the average RGB value of each grid block
for i in range (5):
    for j in range (12):
```

```
            block = img_array[i * block_height:(i + 1) * block_height, j *
block_width:(j + 1) * block_width]
            rgb_values [i, j] = block.mean(axis = (0, 1))

# Calculate (B+R)/G ratio
br_g_ratios = (rgb_values [:, :, 2] + rgb_values [:, :, 0]) / rgb_values [:, :, 1]

# Visualization
colors = ["#FFA500", "#8B0000"]
cmap = LinearSegmentedColormap.from_list ("custom_cmap", colors)

# Create heatmap
plt.figure(figsize = (12, 6))
plt.imshow(br_g_ratios, aspect='auto', cmap=cmap, vmin=1.5, vmax=4)
plt.colorbar(label='(B+R)/G Value')

# Axis configuration
x_values = np.arange(0.05, 3.2, 0.28)
new_x_labels = [f"{x:.1f}" for x in x_values]
y_labels = [1, 2, 3, 4, 5]
plt.xticks(np.arange(len(new_x_labels)), new_x_labels, fontsize=16,
fontweight='bold')
plt.yticks(np.arange(len(y_labels)), y_labels, fontsize=16, fontweight='bold')
plt.xlabel('MBZ Concentration (μM)', fontsize=18, fontweight='bold')
plt.ylabel('Repetition', fontsize=18, fontweight='bold')
plt.title('Heatmap of (B+R)/G forMBZ', fontsize=20, fontweight='bold')
```

```
# Data annotation
for i in range(br_g_ratios.shape[0]):
    for j in range(br_g_ratios.shape[1]):
        plt.text (j, i, f'{br_g_ratios [i, j]:.2f}',
                  ha='center', va='center',
                  color='white' if br_g_ratios [i, j] < 2.7 else 'black',
                  fontsize=14, fontweight='bold')
plt.tight_layout()
plt.show()
```

2 Results and Discussion

2.1 Construction of UiO-66-NH_2@MIP/PCN-224@MIP 3D μPAD sensing platform

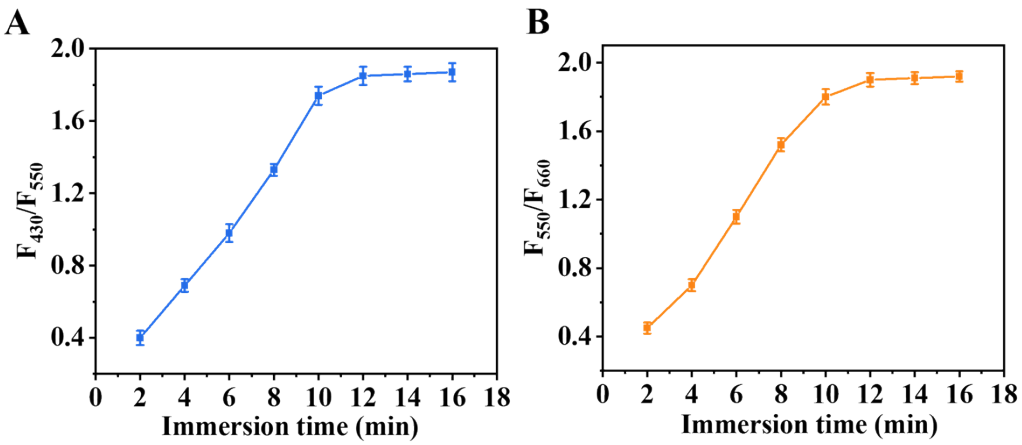

Figure S1 Influence of immersion time of (A) UiO-66-NH_2@MIP sensing unit and (B) PCN-224@MIP sensing unit. Data are presented as mean ± SD (n = 3).

2.2 Characterization

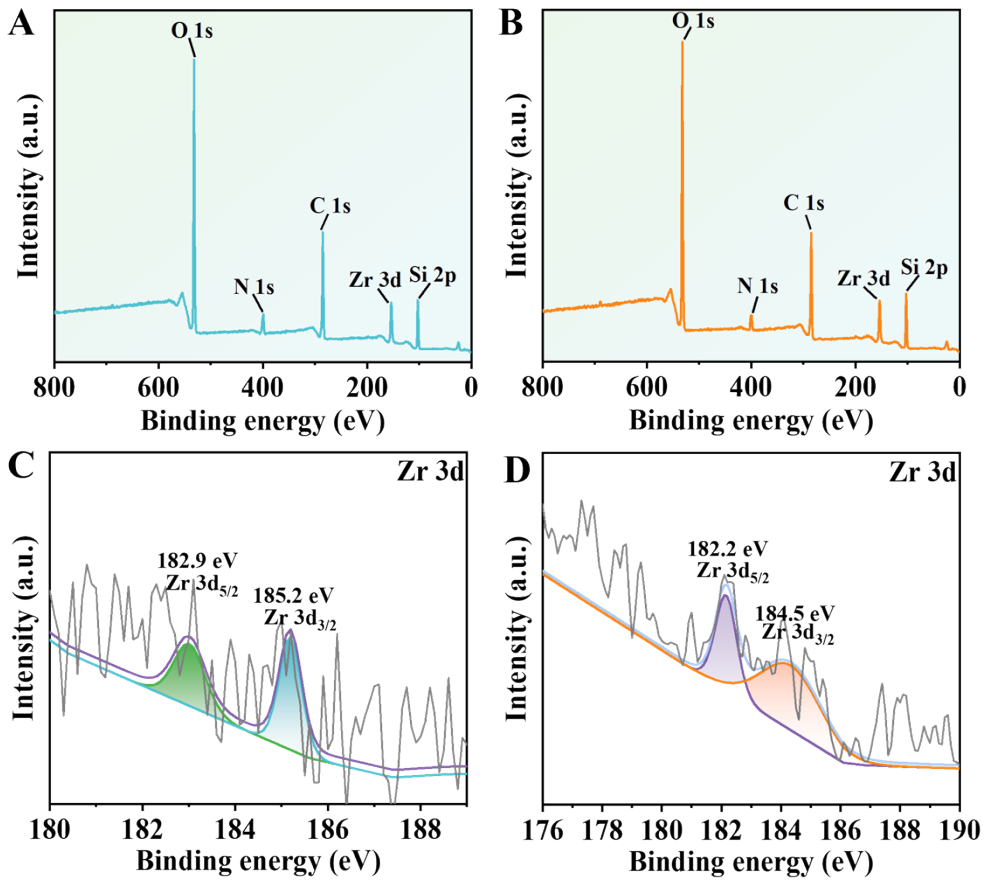

Figure S2 Full XPS spectrum of (A) UiO-66-NH_2@MIP and (B) PCN-224@MIP. Zr XPS spectrum of (C) UiO-66-NH_2@MIP and (D) PCN-224@MIP.

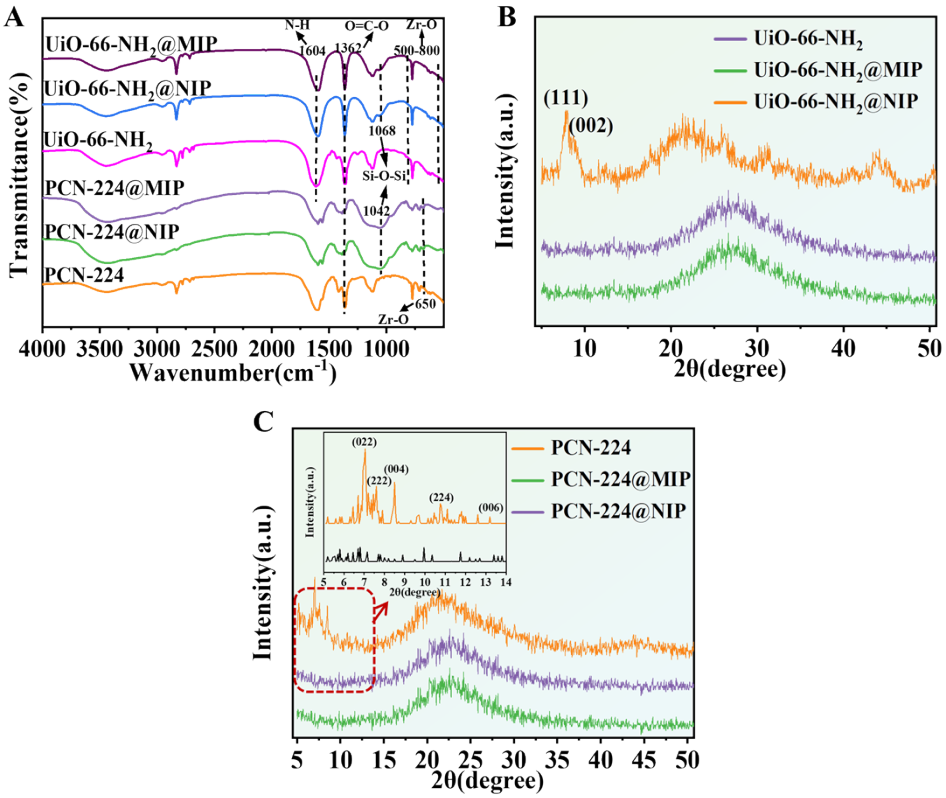

Figure S3 (A) FT-IR spectra of different materials. (B) XRD patterns of UiO-66-NH_2 and UiO-66-NH_2@MIP, UiO-66-NH_2@NIP; (C) XRD patterns of PCN-224 and PCN-224@MIP, PCN-224@NIP.

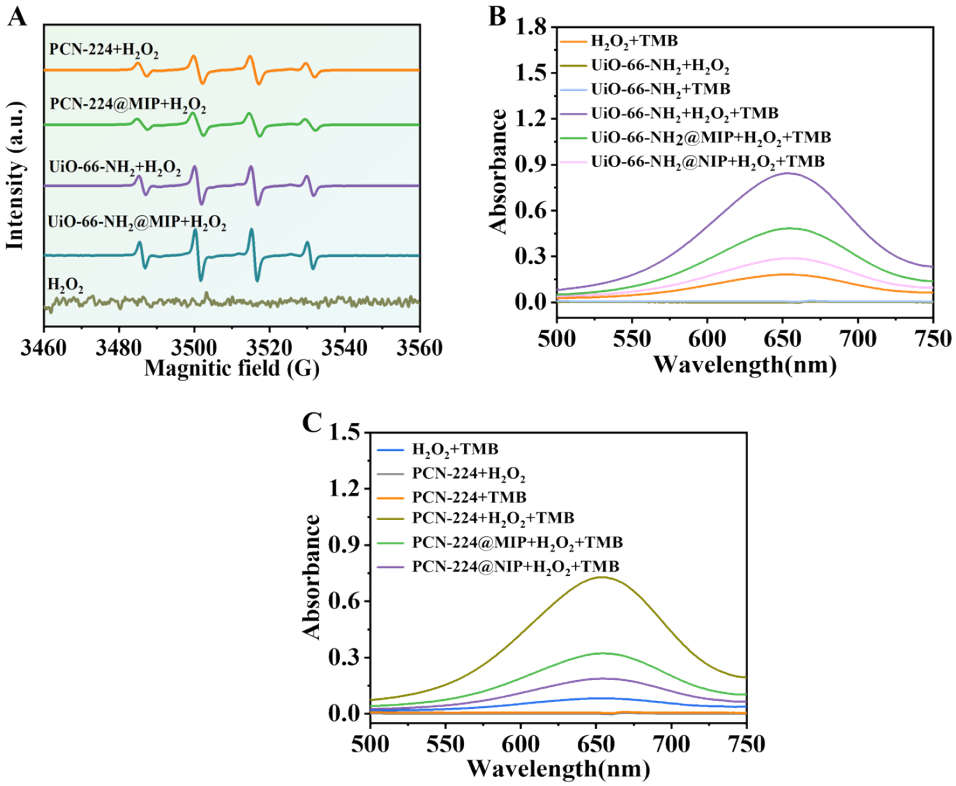

Figure S4 (A) EPR spectra of different reaction systems. (B) and (C) UV-vis spectra of various systems.

2.3 Peroxidase-like properties of materials

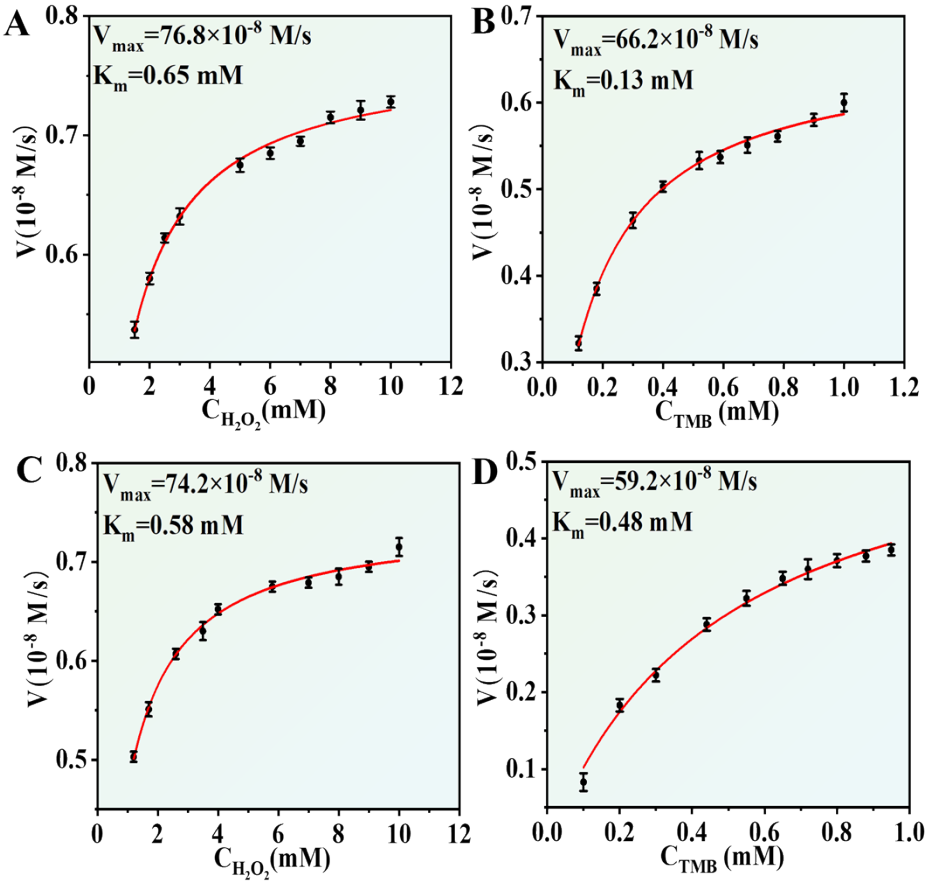

Figure S5 (A) Michaelis-Menten plots of UiO-66-NH_2@MIP activity at fixed 5 mM TMB. (B) Michaelis-Menten plots of UiO-66-NH_2@MIP activity at fixed 0.98 mM H_2O_2. (C) Michaelis-Menten plots of PCN-224@MIP activity at fixed 5 mM TMB. (D) Michaelis-Menten plots of PCN-224@MIP activity at fixed 0.98 mM H_2O_2. Data are presented as mean ± SD (n = 3).

Table S1 Comparison of K_m and V_{max} different nanozymes

Materials	K_m (mM)		V_{max} (10^{-8} M/s)		Reference
	H_2O_2	TMB	H_2O_2	TMB	
Co-MOFs	0.41	0.97	17.6	14.3	[54]
UiO-66(Ce)	-	0.13	-	-	[55]
Co/Fe-MOFs	3.51	5.37	7.63	2.71	[56]
HRP	0.434	10.00	3.7	8.71	[57]
Cu-N-C	19.94	3.76	20.07	75.05	[58]
Pt HN	6.90	0.81	9.90	12.00	[59]
Cu-Ag/rGO	8.62	0.63	7.02	4.26	[60]
Fe-MOF-GOx	2.06	2.84	7.04	10.47	[61]
CP600-6	9.56	0.25	1.31	1.28	[62]
PCN-222(Fe)	13.70	0.17	1.03	0.92	[63]
UiO-66-NH_2@MIP	0.65	0.13	76.8	66.2	This work
PCN-224@MIP	0.58	0.48	74.2	59.2	This work

2.4 Fluorescence sensing mechanism

To rule out potential cross-interference between LMS and MBZ in our dual-channel ratiometric system, control experiments were conducted (Figure S9). Optical cross-talk test: Under 360 nm excitation, a pure MBZ solution at 100× its LOD exhibited negligible fluorescence change at 550 nm. Similarly, under 420 nm

excitation, pure LMS at 100× LOD showed no detectable emission at 550 nm. These results confirm that neither analyte exhibits intrinsic fluorescence within the ox-OPD detection window, effectively ruling out optical cross-talk. Substrate depletion and functional interference test: In the presence of a fixed concentration of LMS, addition of 100× LOD MBZ to the LMS-sensing zone (UiO-66-NH_2@MIP + OPD + H_2O_2) caused no significant change in the 550 nm fluorescence signal under 365 nm excitation. Conversely, when high-concentration LMS was introduced into the MBZ-sensing zone (PCN-224@MIP + OPD + H_2O_2), the 550 nm fluorescence signal remained stable under 420 nm excitation. Given that OPD and H_2O_2 are pre-loaded in excess in both zones, these findings demonstrate that neither analyte non-specifically interferes with the other's recognition or catalytic process, and substrate depletion is not a concern.

In summary, even under worst-case interference conditions (i.e., mutual spiking at 100× LOD), the dual-detection system operates independently, with no measurable cross-talk observed.

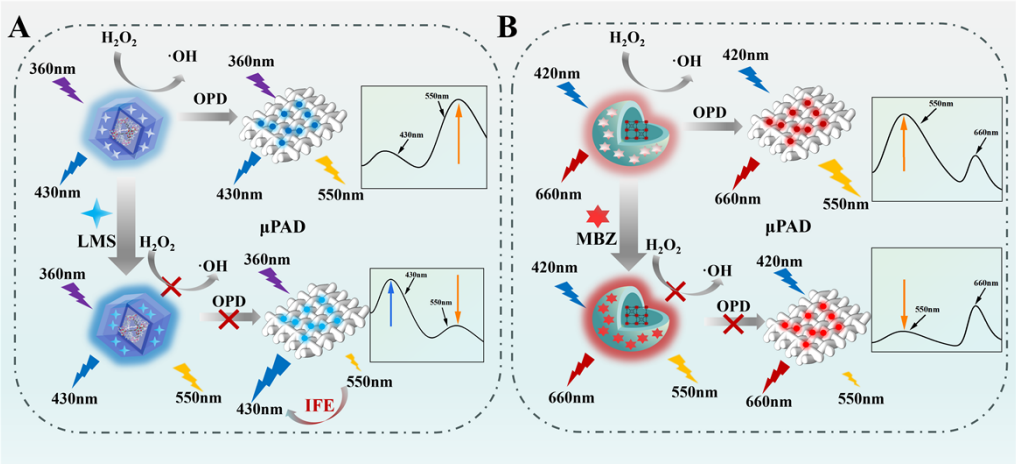

Figure S6 (A) Response process of UiO-66-NH_2@MIP + H_2O_2 + OPD system signal toward LMS. (B) Response process of PCN-224@MIP + H_2O_2 + OPD system signal toward MBZ.

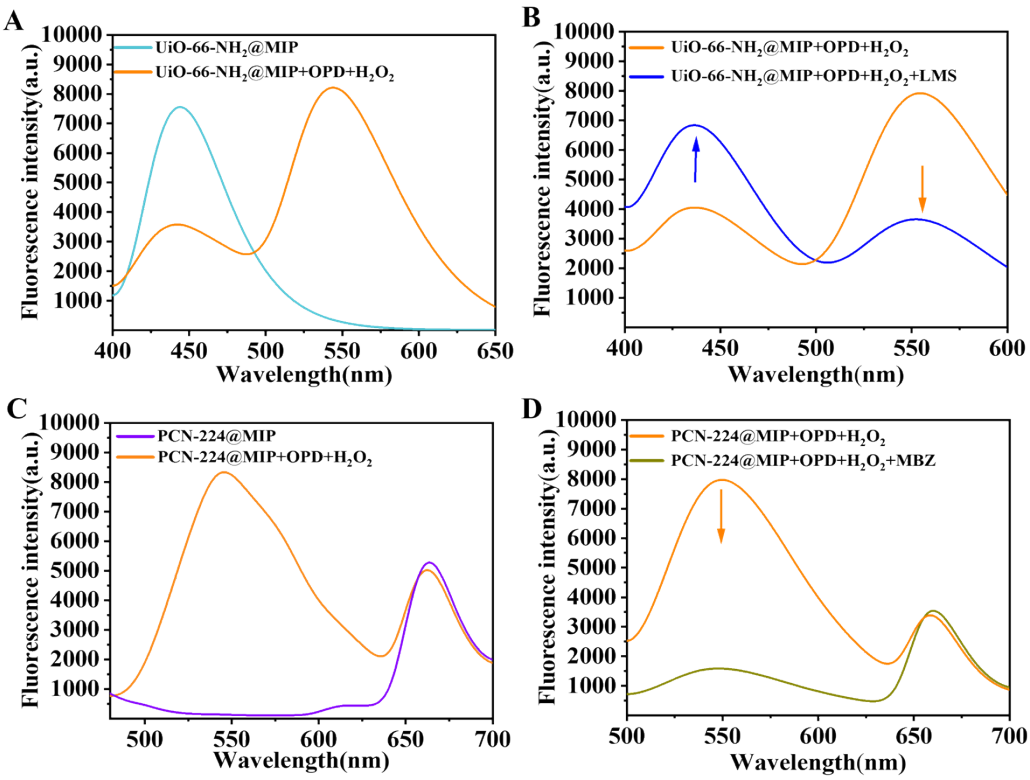

Figure S7 (A) Fluorescence spectra of UiO-66-NH_2@MIP and UiO-66-NH_2@MIP + OPD + H_2O_2 systems. (B) Fluorescence spectra of UiO-66-NH_2@MIP + OPD + H_2O_2 system after adding the LMS. (C) Fluorescence spectra of PCN-224@MIP and PCN-224@MIP + OPD + H_2O_2 systems. (D) Fluorescence spectra of PCN-224@MIP + OPD + H_2O_2 system after adding the MBZ.

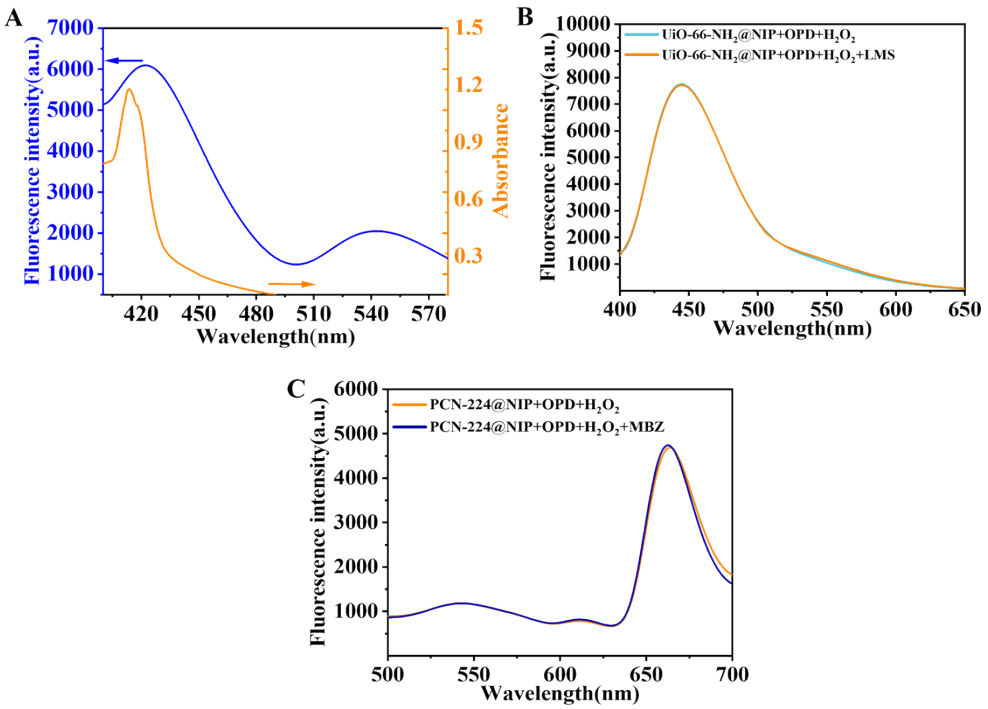

Figure S8 (A) Fluorescence spectra of UiO-66-NH_2@MIP and UV-Vis absorption spectra of ox-OPD. (B) Fluorescence spectra of UiO-66-NH_2@NIP + OPD + H_2O_2 system after adding the LMS. (C) Fluorescence spectra of PCN-224@NIP + OPD + H_2O_2 system after adding the MBZ.

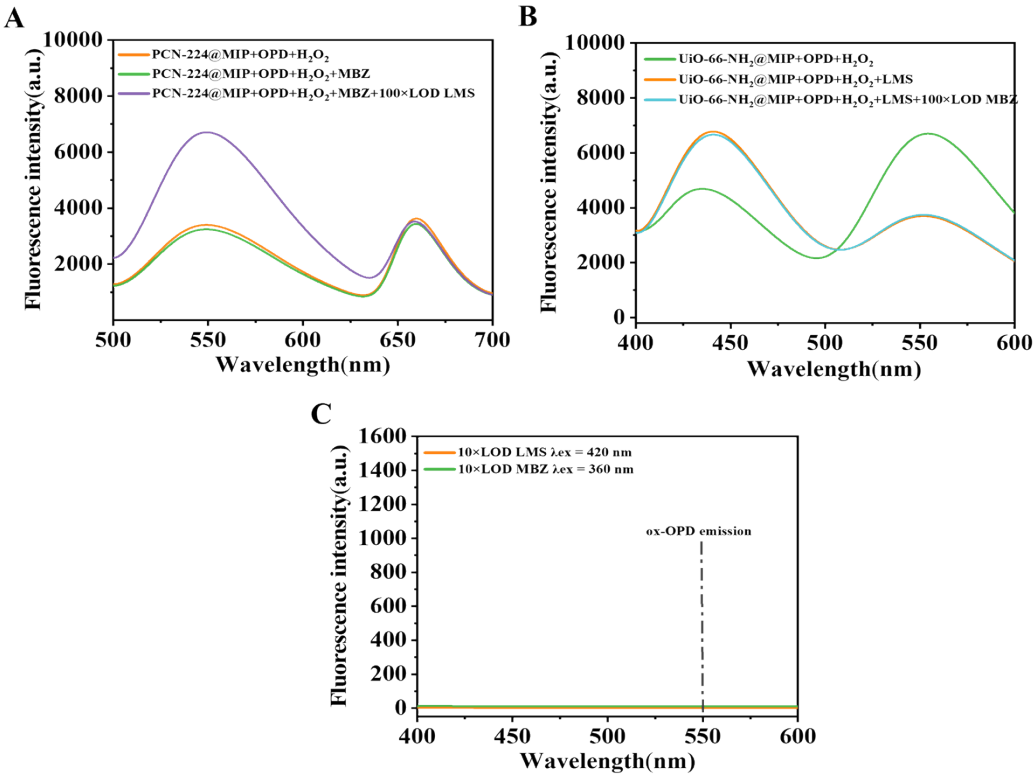

Figure S9 (A) Response of the MBZ-sensing zone to LMS spiked at 100× LOD. (B) Response of the LMS-sensing zone to MBZ spiked at 100× LOD. (C) Fluorescence emission at 550 nm under 365 nm or 420 nm excitation in the presence of high-concentration LMS or MBZ alone.

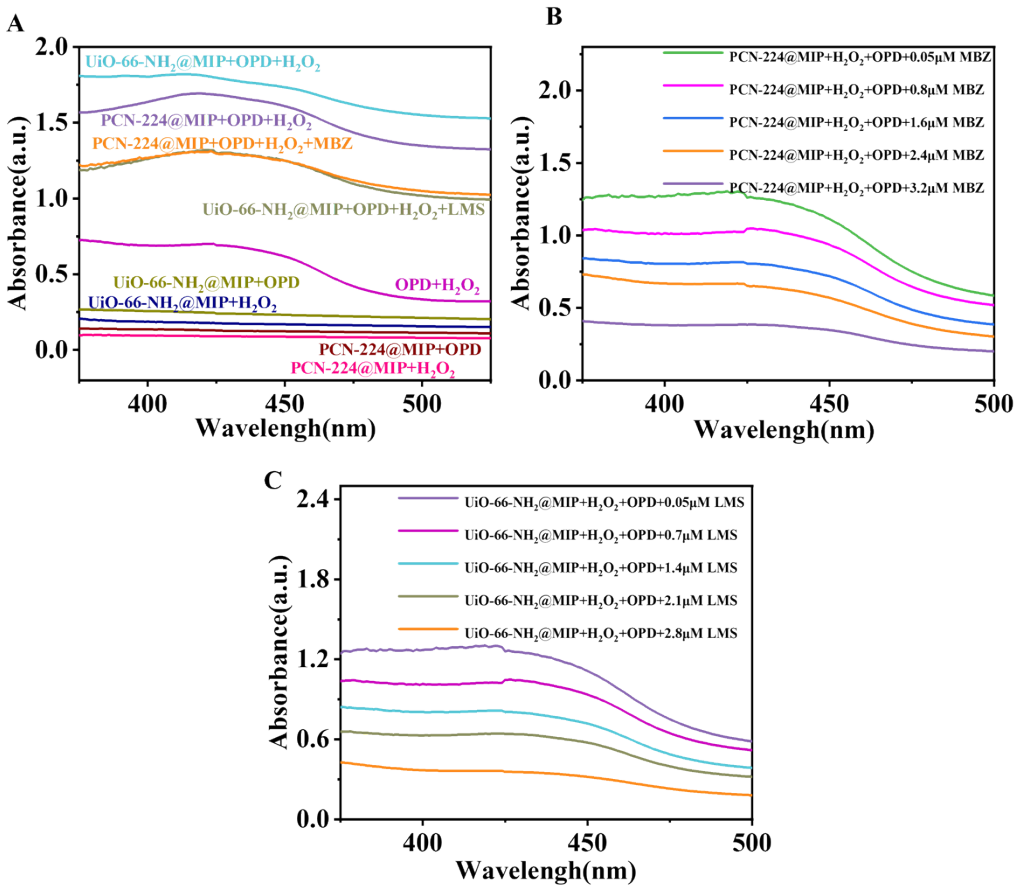

Figure S10 (A) UV-Vis absorption spectra under different reaction conditions. (B) UV-Vis spectra of PCN-224@MIP + H_2O_2 + OPD with increasing MBZ concentrations. (C) UV-Vis spectra of UiO-66-NH_2@MIP + H_2O_2 + OPD with increasing LMS concentrations.

2.5 Optimization of detection conditions

As show in Figure S11A, UiO-66-NH_2@MIP sensing unit exhibited the strongest fluorescence emission at 360 nm excitation, while PCN-224@MIP sensing unit achieved maximum fluorescence intensity at 420 nm excitation (Figure S12A).

The effect of pH in the range of 3.0-8.0 on the fluorescence response efficiency of the sensing system to LMS and MBZ was investigated. As show in Figure S11B and S12B, both systems exhibited optimal fluorescence sensitivity at pH 5.0, where the

F_{430}/F_{550} ratio of the UiO-66-NH_2@MIP sensing unit and the F_{550}/F_{660} ratio of the PCN-224@MIP sensing unit reached their maxima. When the pH value is less than 5.0, the amino groups of MIPs are protonated, which weakens the binding ability between the UiO-66-NH_2@MIP or PCN-224@MIP sensing unit and the template. When the pH value is greater than 5.0, SiO_2 ionizes in an alkaline environment, destroying the structure of the MIPs, thereby reducing the sensitivity of the sensing unit to the template. In addition, the fluorescence response intensity of the UiO-66-NH_2@MIP and PCN-224@MIP sensing units toward the template are higher than those of the UiO-66-NH_2@NIP and PCN-224@NIP sensing units in same pH solutions owing to no imprinted cavities in the non-imprinted polymers.

Under the conditions of pH = 5.0 and excitation wavelengths of 360 nm and 420 nm respectively, the reaction time of UiO-66-NH_2@MIP and PCN-224@MIP sensing units to the templates was optimized by measuring the changes in fluorescence intensity ratio. As shown in Figure S11C and S12C, after the addition of LMS or MBZ, the fluorescence responses of both sensing units changed continuously and stabilized at 6 minutes, indicating that the optimal reaction time for detection was 6 minutes.

To optimize the fluorescence recognition capability of the sensing units for templates, the incubation time was investigated by adding templates to the sensing unit system. Under the conditions of pH = 5.0 and excitation wavelengths of 360 nm and 420 nm respectively, the fluorescence responses of UiO-66-NH_2@MIP and PCN-224@MIP sensing units to 1 μM LMS and MBZ were explored, with the changes in

fluorescence intensity recorded within 8 minutes. As shown in Figure S11D and S12D, the fluorescence intensity ratios of both sensing units in response to their respective templates tended to stabilize within 6 minutes, indicating that the effective recognition of template molecules was completed within 6 minutes. Thus, 6 minutes was selected as the optimal incubation time for subsequent studies. In addition, under the same conditions, the changes in fluorescence intensity of the MIPs sensing units were higher than those of the NIPs sensing units. This is because the imprinted surface of MIPs contains multiple active sites with specific binding affinity for the templates.

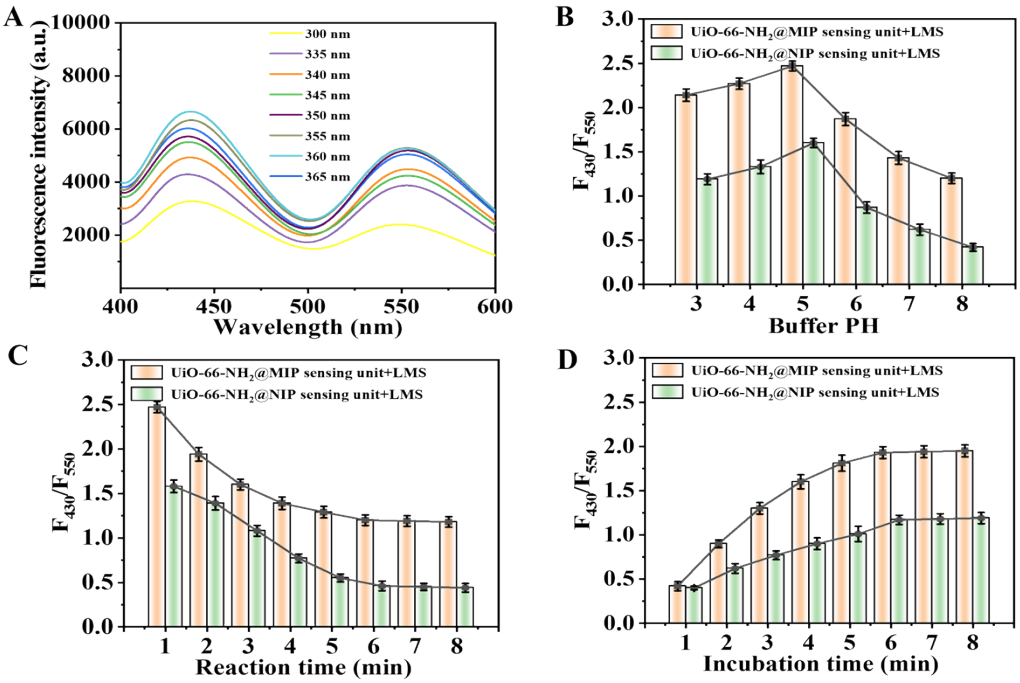

Figure S11 (A) Effect of different excitation wavelengths on UiO-66-NH_2@MIP. (B) Effect of UiO-66-NH_2@MIP/NIP on the fluorescence intensity ratio of LMS under different pH conditions. (C) Change in the fluorescence intensity ratio of UiO-66-NH_2@MIP/NIP toward LMS at different response times. (D) Change in the fluorescence intensity ratio of UiO-66-NH_2@MIP/NIP toward LMS at different incubation times. Data are presented as mean ± SD (n

= 3).

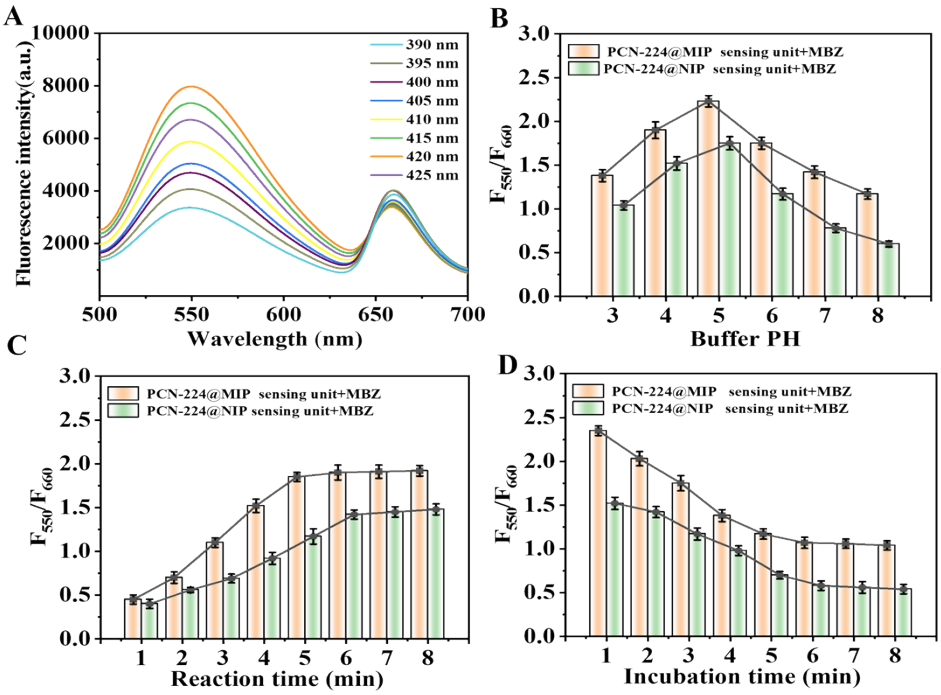

Figure S12 (A) Effect of different excitation wavelengths on PCN-224@MIP. (B) Effect of PCN-224@MIP@MIP/NIP on the fluorescence intensity ratio of LMS under different pH conditions. (C) Change in the fluorescence intensity ratio of PCN-224@MIP@MIP/NIP toward LMS at different response times. (D) Change in the fluorescence intensity ratio of PCN-224@MIP@MIP/NIP toward LMS at different incubation times. Data are presented as mean ± SD (n = 3).

2.6 Fluorescence analytical performance of nanozyme imprinted 3D μPAD sensors for LMS and MBZ.

As shown in Figure S13A and S13B, the UiO-66-NH_2@NIP and PCN-224@NIP sensing units show weaker fluorescence response than MIP sensing units. As shown in Figure S13B and S13D, the linear correlation coefficients (R^2 values of 0.953 and 0.928) between

the fluorescence intensity ratio of NIPs sensing units and LMS or MBZ concentrations were significantly lower than those of the corresponding MIPs sensing units, the imprinting effect was evaluated using the imprinting factor IF = K_{MIP}/K_{NIP} (where K_{MIP} and K_{NIP} are the linear slopes of the working equations for MIP and NIP, respectively). The results showed that the IF values for LMS and MBZ were calculated as 3.45 and 3.22, which indicated that UiO-66-NH_2@MIP and PCN-224@MIP sensing units could successfully recognize the template molecules. In conclusion, the UiO-66-NH_2@MIP/PCN-224@MIP 3D μPAD sensor can achieve ultra-high sensitivity simultaneous detection of LMS and MBZ.

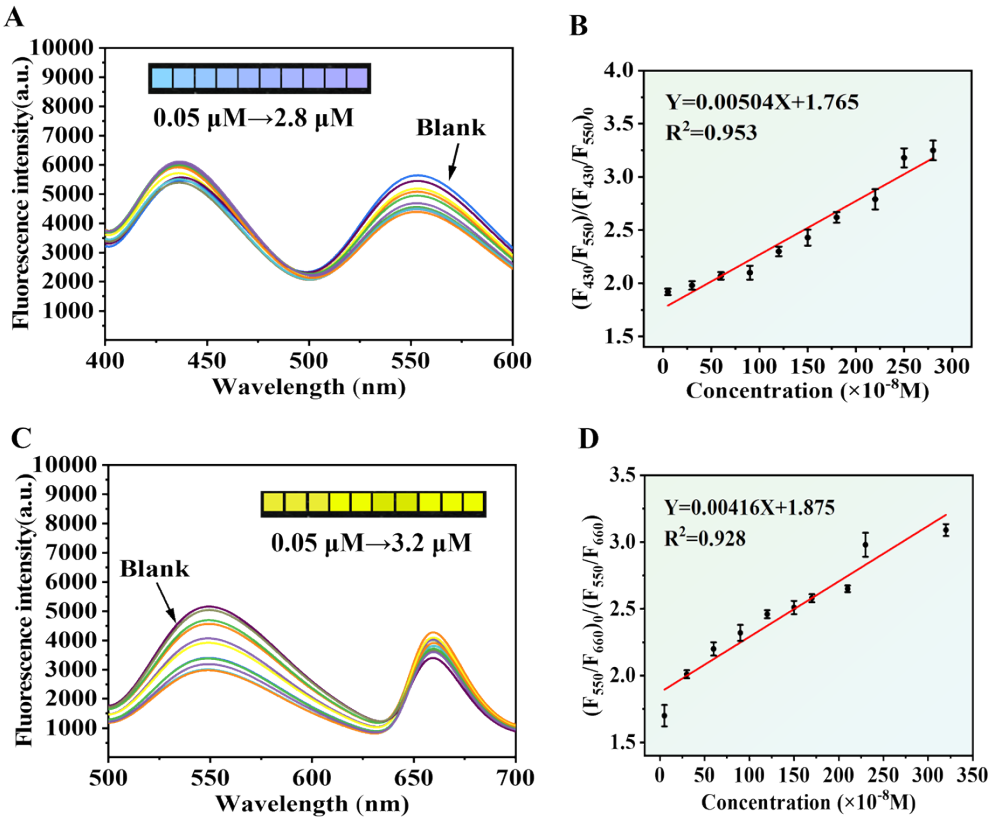

Figure S13 (A) Fluorescence spectra of UiO-66-NH_2@NIP sensing unit + H_2O_2 + OPD system with different levels of LMS. (B) Correlation of $(F_{430}/F_{550})/(F_{430}/F_{550})_0$ to the level of LMS. (C)

Fluorescence spectra of PCN-224@NIP sensing unit + H_2O_2 + OPD system with different levels of MBZ. (D) Correlation of $(F_{550}/F_{660})_0/(F_{550}/F_{660})$ to the level of MBZ. Data are presented as mean ± SD (n = 3).

2.7 Performance robustness and analytical reliability

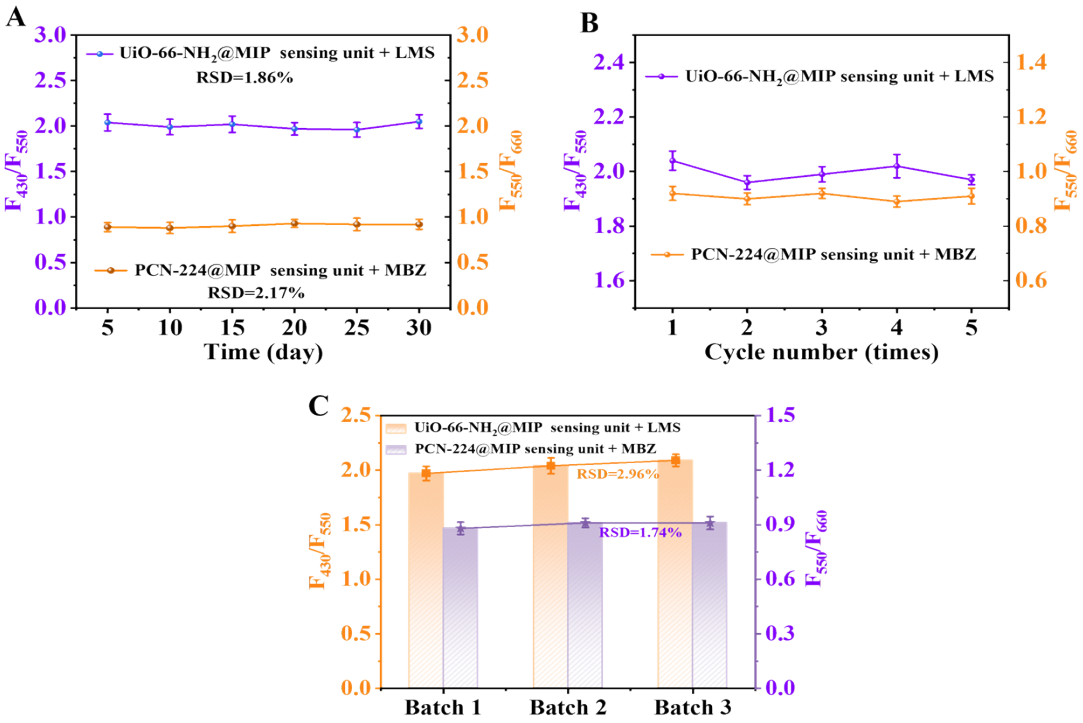

Figure S14 (A) Stability and (B) reproducibility and (C) Inter-batch reproducibility of the UiO-66-NH_2@MIP or PCN-224@MIP sensing unit for determination of LMS or MBZ. Data are presented as mean ± SD (n = 3).

References

[51] P. Jia, K. Yang, J. Hou, Y. Cao, X. Wang and L. Wang, *Journal of Hazardous Materials*, 2021, **408**, 124469.

[52] J. Zhang, L. Chang, R. Hao, G. Zhang, T. Liu, Z. Li, T. Wang and L. Zeng, *Chemical Engineering Journal*, 2023, **474**, 145485.

[53] P. Gao, P. Zhang, Y. Guo, Z. He, Y. Dong, Y. Tang, F. Guan, T. Zhang and K. Xie, *Foods*, 2021, **10**, 2841.

[54] H. Wan, Y. Wang, J. Chen, H. M. Meng and Z. Li, *Mikrochim Acta*, 2021, **188**, 130.

[55] Y. Zhang, X. Zeng, X. Jiang, H. Chen and Z. Long, *Microchemical Journal*, 2019, **149**, 103967.

[56] X. L. Zhao, J. L. Liu, F. T. Xie, T. Yang, R. Hu and Y. H. Yang, *Spectrochimica Acta Part A: Molecular and Biomolecular Spectroscopy*, 2021, **262**, 120117.

[57] L. Gao, J. Zhuang, L. Nie, J. Zhang, Y. Zhang, N. Gu, T. Wang, J. Feng, D. Yang, S. Perrett and X. Yan, *Nature nanotechnology*, 2007, **2**, 577-583.

[58] Y. Wu, J. Wu, L. Jiao, W. Xu, H. Wang, X. Wei, W. Gu, G. Ren, N. Zhang, Q. Zhang, L. Huang, L. Gu and C. Zhu, *Analytical Chemistry*, 2020, **92**, 3373-3379.

[59] C. Ge, R. Wu, Y. Chong, G. Fang, X. Jiang, Y. Pan, C. Chen and J. J. Yin, *Advanced Functional Materials*, 2018, **28**, 1801484.

[60] G. Darabdhara, B. Sharma, M. R. Das, R. Boukherroub and S. Szunerits, *Sensors and Actuators B: Chemical*, 2017, **238**, 842-851.

[61] W. Xu, L. Jiao, H. Yan, Y. Wu, L. Chen, W. Gu, D. Du, Y. Lin and C. Zhu,

ACS applied materials & interfaces, 2019, **11**, 22096-22101.

[62] Z. Lou, S. Zhao, Q. Wang and H. Wei, *Analytical chemistry*, 2019, **91**, 15267-15274.

[63] Y. Wang, T. Li and H. Wei, *Analytical Chemistry*, 2023, **95**, 10105-10109.